Analysis on SiO_2 Particle Generation and Deposition Using Tube Furnace Reactor

Kyo-Seon Kim
Dept. of Chemical Engineering, Kangwon National University, Chunchon, Kangwon-Do 200-701, Korea

The combined phenomena of SiO_2 particle generation and deposition were analyzed theoretically and experimentally in a tubular flow reactor. The deposition tube was directly connected to a high-temperature tube furnace reactor by a flange and the deposition characteristics of SiO_2 particles were measured. The $SiCl_4$ conversion and deposition efficiencies were calculated, solving the mass and energy balance equations and the aerosol dynamic equation in the tubular flow reactor. Effects of process variables such as furnace set temperature, inlet $SiCl_4$ concentration and total gas-flow rate were examined. Experimental results agreed closely with theoretical prediction. Effects of natural convection are significant at low gas-flow rate. Tube wall temperature profiles inside the deposition tube were proposed for uniform coating of SiO_2 particles. The study shows that the tube furnace reactor can be used to coat the inside wall of the deposition tube with ultrafine particles uniformly by adjusting tube wall temperature profiles.

Introduction

The tube furnace reactor has been used frequently to analyze ultrafine particle generation because of its simplicity. Ultrafine particles such as SiC (Chen et al., 1989), AlN (Kimura et al., 1989), TiO_2 (Suyama and Kato, 1985; Morooka et al., 1987), SiO_2 and Al_2O_3 (Okuyama et al., 1986, 1990) were experimentally produced in a tube furnace reactor. Okuyama et al. (1986) measured the size distribution of metal oxide particles produced by a thermal decomposition of alkoxide vapors in a tubular furnace and compared the experimental results with the solutions of the discrete-continuous general dynamic equation for aerosols. Okuyama et al. (1990) included seed particles in a similar analysis. Pratsinis et al. (1986) predicted the aerosol product characteristics in several aerosol reactors including a tubular flow reactor. Akhtar et al. (1991, 1994) produced TiO_2 powder by oxidation and hydrolysis of $TiCl_4$ using a tubular flow reactor. The experimental observations on particle-size distribution were compared with theoretical predictions by a sectional technique.

Most of these analyses in tube furnace reactors are limited to the particle generation and growth just in the reaction zone and do not include the particle transport in the cylindrical flow. The modified chemical vapor deposition (MCVD) process for optical fiber preform fabrication includes the silica particle formation and transport in nonisothermal cylindrical flow (MacChesney et al., 1974; Walker et al., 1980; Nagel et al., 1982; Kim and Pratisinis, 1988). Simpkins et al. (1979) showed that thermophoresis is the major transport mechanism of particles in MCVD. Walker et al. (1979, 1980) analyzed the particle transport in laminar tube flows without including the oxidation kinetics and aerosol dynamics. Kim and Pratsinis (1988) proposed model equations in MCVD including mass and energy balance equations and the aerosol dynamic equation. They solved the model equations simultaneously, assuming that the aerosol size distribution is lognormal and showed that the overall deposition efficiencies by numerical predictions are in close agreement with the experimental observations in MCVD.

In this study, the model equations proposed by Kim and Pratsinis (1988) for MCVD were extended and applied to the experimental tube furnace reactor and deposition tube. The concurrent phenomena of chemical oxidation, SiO_2 particle generation, and deposition in a nonisothermal tubular flow reactor were analyzed theoretically and experimentally. The mass and energy balance equations and the aerosol dynamic equation in a tubular flow reactor were solved simultaneously and the $SiCl_4$ conversion and deposition efficiencies were calculated. In experiments, a pyrex tube (deposition zone) was directly connected to the tube furnace reactor (reaction zone). Silica particles are formed at high temperature by oxidation of $SiCl_4$ in the tube furnace and are deposited onto the pyrex tube wall. The unit cells were packed inside the deposition tube and the amounts of SiO_2 particles deposited were mea-

sured along the axial distance. The deposition efficiencies by experiments were compared with the theoretical predictions. The effects of process variables such as furnace set temperature, inlet $SiCl_4$ concentration, and total gas-flow rate on $SiCl_4$ conversion and deposition efficiency were investigated. The possible application of tube furnace reactor for uniform coating of SiO_2 particles in a deposition tube was also proposed.

Theoretical Approach

Model equations such as energy and $SiCl_4$ balance equations and aerosol dynamic equation of SiO_2 particles were proposed and solved in a tubular flow reactor. The total molar flow rate of the gas stream is independent of chemical reaction, because each molecule of $SiCl_4$ and O_2 reacts to form two molecules of Cl_2. Oxygen is supplied in excess and the oxidation rate of $SiCl_4$ is first-order with respect to $SiCl_4$ independent of O_2 concentration (Powers, 1978; French et al., 1978). The effects of chemical reaction rate and aerosol generation rate, diffusion, coagulation, and thermophoresis of aerosols were included in the aerosol dynamic equation. The effects of heat and mass transfer in axial direction were neglected (P_{eh} & $P_{em} \gg 1$), and the effect of natural convection was assumed to be negligible (Kays and Perkins, 1985). The effects of aerosol loading on transport equations were also neglected. The gas properties and the gas velocities were calculated at the average gas temperatures.

Based on the assumptions above, the energy balance and mass balance of $SiCl_4$ can be written as Eq. 1 and Eq. 2, respectively (Kim and Pratsinis, 1988)

$$u\frac{\partial T}{\partial z} = \frac{\alpha}{r}\frac{\partial}{\partial r}\left(r\frac{\partial T}{\partial r}\right) - \Delta H\,\mathrm{RXN}/\rho C_p \tag{1}$$

$$u\frac{\partial C}{\partial z} = \frac{1}{r}\frac{\partial}{\partial r}\left(Dr\frac{\partial C}{\partial r}\right) - \mathrm{RXN} \tag{2}$$

The effects of radial diffusion and oxidation reaction on heat and $SiCl_4$ balance equations are written on the righthand side of Eq. 1 and Eq. 2, respectively. The $SiCl_4$ oxidation rate (RXN) was expressed as $\mathrm{RXN} = k_0 \exp(-E/RT)C$ ($k_0 = 1.7 \times 10^{14}$ s^{-1}, $E = 402$ kJ/mol, $\Delta H = -251$ kJ/mol) (Powers, 1978).

The SiO_2 particle-size distribution changes along the reactor by particle generation, diffusion, thermophoresis, coagulation, and convection of particles. The aerosol dynamic equation for particles in the size range of $v \sim v + dv$ can be written as (Friedlander, 1977; Brock, 1983; Seinfeld, 1986)

$$u\frac{\partial n}{\partial z} = \frac{1}{r}\frac{\partial}{\partial r}\left[r\left(D_p\frac{\partial n}{\partial r} + nK\nu\frac{\partial \ln T}{\partial r}\right)\right] + \frac{1}{2}\int_{v^*}^{v}\beta(v', v-v')n(v',r,z)n(v-v',r,z)dv' - \int_{v^*}^{\infty}\beta(v,v')n(v,r,z)n(v',r,z)dv' + \mathrm{RXN}\,\delta(v-v^*)N_{av} \tag{3}$$

The first and second terms on the righthand side of Eq. 3 show the transport rates in radial direction by diffusion and thermophoresis, respectively, and β is the collision frequency function of particles. The last term on the righthand side of Eq. 3 is the particle generation rate by oxidation of $SiCl_4$ and v^* is the volume of SiO_2 monomer. The aerosol particles along the reactor were assumed to have log-normal size distribution and the first three moments of aerosol particles (M_0, M_1, M_2) are enough to express the aerosol concentration (M_0), average particle size [$v_g = M_1^2/(M_0^3M_2)^{1/2}$], and standard deviation [σ, $\ln^2\sigma = \ln(M_0M_2/M_1^2)/9$]. The governing equations for the first three moments in MCVD were derived from the aerosol dynamic equation by Kim and Pratsinis (1988). In this study, the governing equations for the first three moments in MCVD were applied for the analysis in the cylindrical tubular flow reactor. The same initial and boundary conditions for T, C, M_0, M_1 and M_2 in MCVD (Kim and Pratsinis, 1988) were applied besides the boundary condition for T at $r = R$. The tube wall temperature was measured along the axial distance by thermocouple and the interpolated $T_w(z)$ was used as the boundary condition for T at $r = R$.

The partial differential equations for T, C, M_0, M_1 and M_2 were converted into ordinary differential equations (ODEs) by applying the method of lines (Anderson et al., 1984) and the ODEs were solved simultaneously along the reactor by DGEAR subroutine (IMSL, 1980). The $SiCl_4$ conversion and average particle size of SiO_2 particles were calculated by using mixing cup average properties (Pratsinis et al., 1986).

Experimental Description

The experimental apparatus is shown in Figure 1. The oxygen gas, after passing through the silica-gel to remove moisture, was supplied to the frit-bubbler where $SiCl_4$ is vaporized. The storage tank of $SiCl_4$ was installed on top of the frit-bubbler and the level of $SiCl_4$ in the frit-bubbler was kept constant by adjusting the valve from the storage tank. The temperature in the frit-bubbler was controlled to keep the $SiCl_4$ vapor pressure constant. The line from frit-bubbler to the tube furnace was heated by heating tape to prevent the condensation of $SiCl_4$ vapor. The excess oxygen was dried and supplied to the tube furnace through another line. The

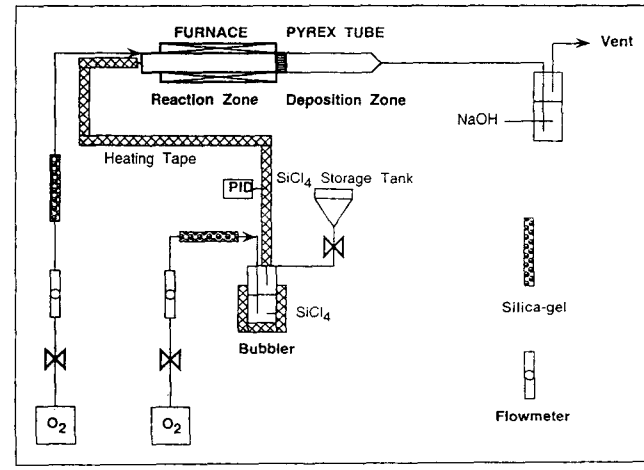

Figure 1. Experimental apparatus.

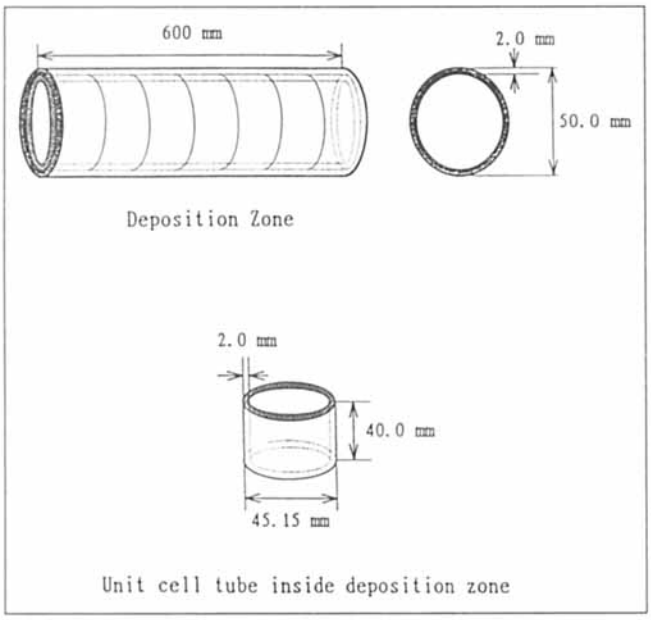

Figure 2. Unit cells to measure the deposition efficiencies in deposition tube.

gas stream was heated in a tube furnace reactor (reaction zone) and the $SiCl_4$ was oxidized at high temperature to form SiO_2 particles. The pyrex tube of the same diameter (deposition zone) was connected to the tube furnace reactor by a flange. The wall temperature of the pyrex tube was lower than the gas stream temperature, and the SiO_2 particles formed in the reaction zone were deposited onto the pyrex tube by thermophoresis. To analyze the deposition characteristics in the deposition zone, segments of a glass tube, which were referred to as unit cells, were packed inside the deposition tube, to be in close contact with the inner wall of deposition tube and to be detachable easily after deposition (Figure 2). Cells composed of 15 units were packed in a 60-cm deposition tube. At first, only oxygen without $SiCl_4$ was supplied for 2 h to stabilize the tube wall temperatures in both reaction and deposition zones. $SiCl_4$ was supplied after the temperature in the reactor reached the steady state. The weights of SiO_2 particles deposited onto the unit cells were measured by weighing the unit cells before and after deposition. The cumulative deposition efficiency of SiO_2 particles along the reactor length was expressed as a function of axial distance by summing up the deposition efficiencies of unit cells. In these experiments, the standard conditions for experimental variables were set as follows: total gas-flow rate: 4 L/min, inlet $SiCl_4$ concentration: 0.5 mol %, and tube wall temperature: 1,300°C. To investigate the effects of experimental variables on deposition efficiencies, total gas-flow rate has changed from 2 to 5 L/min (STP) and inlet $SiCl_4$ concentration from 0.5 mol % to 5 mol %, and tube wall temperature from 1,200°C to 1,400°C.

Results and Discussion

Tube wall temperatures in reaction zone and deposition zone

In these experiments, a 62-cm long tube is in the tube furnace reactor where oxidation reaction of $SiCl_4$ takes place at high temperature and the length of the pyrex tube where deposition of SiO_2 particles takes place is 60 cm. The reaction zone is defined in $0 \le z < 62$, and the deposition zone is in $62 \le z \le 122$. The inside tube wall temperature (T_w) in reaction and deposition zones was measured by a flexible thermocouple (K-type, Cole-Parmer) as a function of axial distance (z). To reduce the radiation effect at high temperature, the shielded thermocouple was used. Figures 3 and 4 show the measured wall temperature profiles in reaction zone and deposition zone, respectively, for various furnace set temperatures with total gas-flow rate of 4 L/min. The tube wall temperature in the reaction zone increases as a quadratic function of z for $0 \le z \le 20$, reaches the furnace set temperature for $20 < z \le 40$ where the tube wall is heated, and decreases as a quadratic function again for $40 < z \le 62$. The tube wall temperature in the deposition zone also decreases as a quadratic function along the axial distance ($62 < z \le 122$). The tube wall temperature profiles for various furnace set temperatures were approximated in quadratic function by curve fitting (Table 1), which were used as the boundary conditions for gas temperature at the tube wall in numerical simulation.

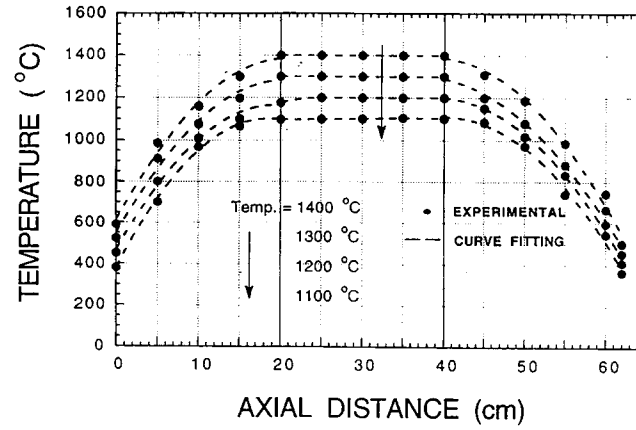

Figure 3. Wall temperature profiles in reaction zone for various furnace set temperatures.

Evolutions of T, C and M_1 profiles along the reactor

Gas temperature profiles computed at standard conditions

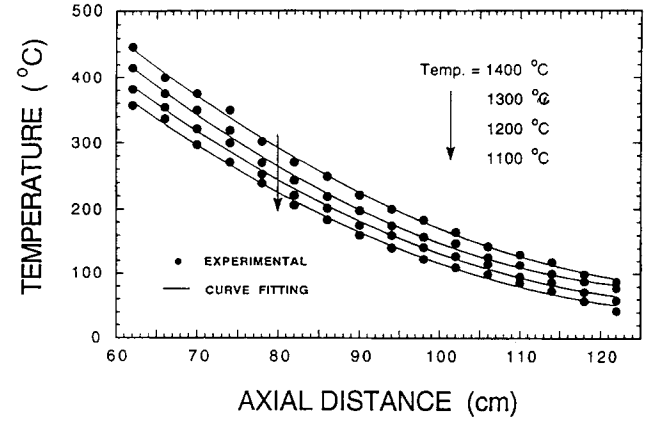

Figure 4. Wall temperature profiles in deposition zone for various furnace set temperatures.

Table 1. Approximated Tube Wall Temperatures for Various Furnace Set Temperatures

T_{ws} \ z	$0 \le z \le 20$	$20 < z \le 40$	$40 < z \le 62$	$62 < z \le 122$
1,200°C	$-1.90\ z^2 + 73.00\ z + 736.65$	1,200°C	$-1.84\ z^2 + 149.28\ z - 1{,}559.74$	$0.061\ z^2 - 16.54\ z + 1{,}450.97$
1,300°C	$-1.77\ z^2 + 72.24\ z + 818.71$	1,300°C	$-1.72\ z^2 + 134.96\ z - 1{,}093.51$	$0.068\ z^2 - 18.02\ z + 1{,}545.23$
1,400°C	$-1.79\ z^2 + 74.45\ z + 884.95$	1,400°C	$-2.11\ z^2 + 172.01\ z - 1{,}849.38$	$0.061\ z^2 - 17.07\ z + 1{,}541.53$

are shown in Figure 5 for various axial distances. The gas temperature profiles are very steep at the beginning of the reactor ($z = 4$, 10), where the gas stream is heated quickly while it becomes less steep as reactor length increases ($20 \le z \le 40$) where the gas temperature reaches the furnace set temperature. As the tube wall temperature becomes lower than gas temperature ($z = 50$, 60, 70, 80), the gas stream is cooled and the gas temperature reaches the tube wall temperature at $z = 120$. Figure 6 shows the dimensionless $SiCl_4$ concentration profiles along the reactor under standard conditions. For $z \le 10$, the gas temperature is not high enough for significant $SiCl_4$ oxidation reaction to take place. The gas temperature is raised substantially downstream of the reaction zone ($20 \le z \le 62$), and most of the inlet $SiCl_4$ is oxidized. Figure 7 shows the dimensionless SiO_2 particle volume profiles ($M_1/C_iN_{av}v^*$) along the reactor at standard conditions. At the beginning of the reactor, the particle volume increases near the tube wall ($r/R = 1$), where the gas temperature is high and the oxidation reaction is fairly fast. As $SiCl_4$ is oxidized first near the tube wall, the $SiCl_4$ con-

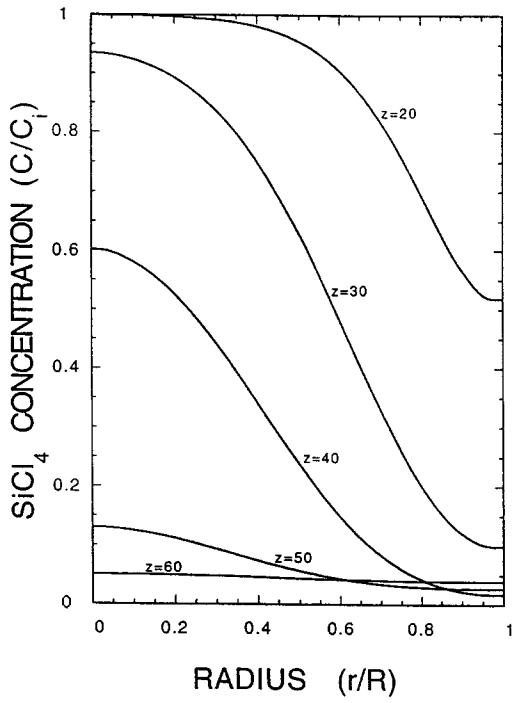

Figure 6. Dimensionless $SiCl_4$ concentration profiles inside the reactor as a function of radius for various axial distances.

T_{ws} = 1,300°C; C_i = 0.5 mol %; Q = 4L/min.

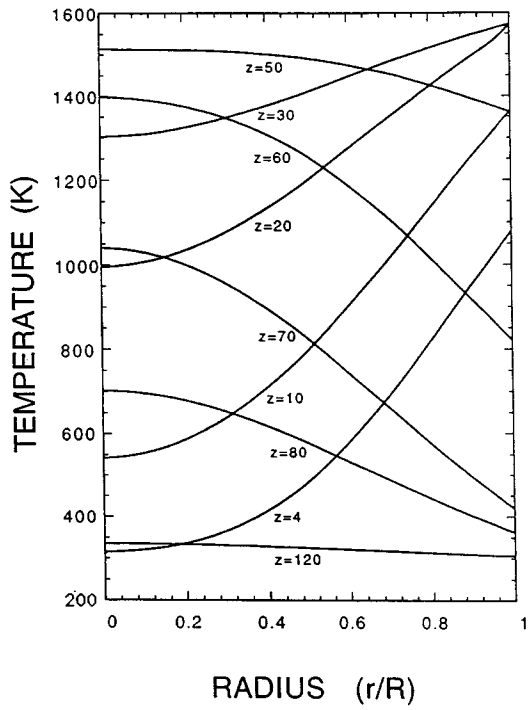

Figure 5. Gas temperature profiles inside the reactor as a function of radius for various axial distances.

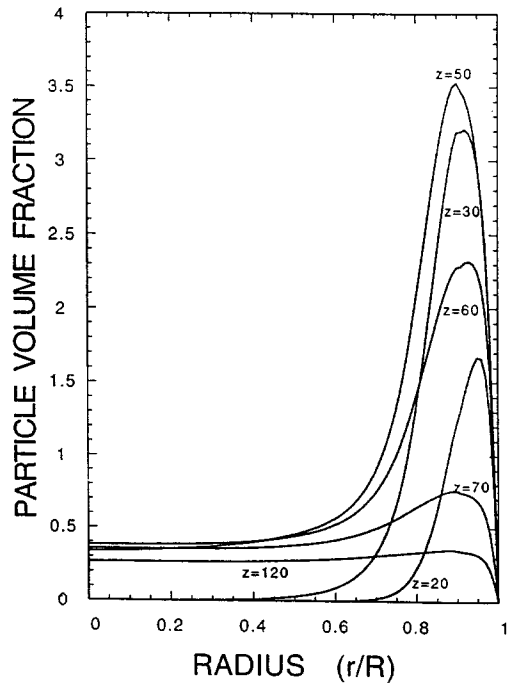

Figure 7. Dimensionless SiO_2 particle volume profiles inside the reactor as a function of radius for various axial distances.

T_{ws} = 1,300°C; C_i = 0.5 mol %; Q = 4L/min.

centration near the tube wall is lower than near the centerline, and $SiCl_4$ diffuses from the centerline toward the region near the tube wall where it reacts to form SiO_2 particles. As a result, further downstream ($20 \leq z \leq 60$), most SiO_2 is present adjacent to the tube wall ($r/R > 0.7$). In the reaction zone, silica particles accumulated near the tube wall by the combined effects of $SiCl_4$ diffusion and oxidation reaction. The dimensionless SiO_2 particle volume is greater than unity near the tube wall (such as the dimensionless particle volume $\fallingdotseq 3.5$ at $z = 50$, and $r/R = 0.9$), while it is smaller than 0.5 near the centerline. As the gas stream is cooled down from the end of the reaction zone ($z > 40$), these particles are deposited on the inside tube wall by thermophoresis and the dimensionless particle volume decreases.

Effects of furnace set temperature on deposition efficiencies

The overall deposition efficiency from the beginning of reaction zone (E_D) and the deposition efficiencies in deposition zone by theoretical predictions ($E_{DZ,\text{the}}$) and by experiments ($E_{DZ,\text{exp}}$) are defined, respectively, as

$$E_D = \frac{\int_0^z (\text{amount of } SiO_2 \text{ particles deposited})\, dz}{(\text{amount of } SiO_2 \text{ particles fully converted by inlet } SiCl_4)} \quad (4)$$

$$E_{DZ,\text{the}} = \frac{\int_{62}^z (\text{amount of } SiO_2 \text{ particles deposited})\, dz}{(\text{amount of } SiO_2 \text{ particles fully converted by inlet } SiCl_4)} \quad (5)$$

$$E_{DZ,\text{exp}} = \sum_{i=1}^{i} \frac{(\text{amount of } SiO_2 \text{ particles deposited on } i\text{th unit cell})}{(\text{amount of } SiO_2 \text{ particles fully converted by inlet } SiCl_4)} \quad (6)$$

The $E_{DZ,\text{the}}$'s were compared with the $E_{DZ,\text{exp}}$'s, changing the conditions of process variables.

The $SiCl_4$ conversion and deposition efficiency (E_D) for furnace set temperature of 1,200°C and 1,300°C were shown in Figure 8. At 1,300°C, the $SiCl_4$ conversion increases rapidly for $25 \leq z \leq 50$, but the $SiCl_4$ conversion doesn't increase beyond for $z \geq 55$ because no more oxidation takes place at low temperature and the final conversion is about 93%. SiO_2 particles are deposited onto the tube wall by thermophoresis while the gas stream is cooled, and the deposition efficiency starts to increase from $z = 40$. The overall deposition efficiency at 1,300°C is about 62%. At furnace set temperature of 1,200°C, the overall deposition efficiency is just about 25% because overall $SiCl_4$ conversion is incomplete ($\fallingdotseq 40\%$) at low temperature. The theoretical deposition efficiencies in the deposition zone ($E_{DZ,\text{the}}$) were compared with the experimental results ($E_{DZ,\text{exp}}$) in Figure 9 for various furnace set temperatures. The deposition efficiencies in the deposition zone are low at 1,200°C because of low $SiCl_4$ conversion. As the furnace set temperature increases from 1,300°C to 1,400°C, the gas stream is heated to higher temperature and the $E_{DZ,\text{exp}}$ increases from 40% to 43% because thermophoretic deposition increases. The results of $E_{DZ,\text{the}}$ are in good agreement with $E_{DZ,\text{exp}}$ for various furnace set temperatures. It is believed that some particles were pushed towards the tube center by natural convection during heat transfer in the reaction zone and these particles are not easily deposited at the beginning of the deposition zone (Kim and Pratsinis, 1988). The effects of natural convection are not included in theoretical analysis and, as a result, $E_{DZ,\text{exp}}$

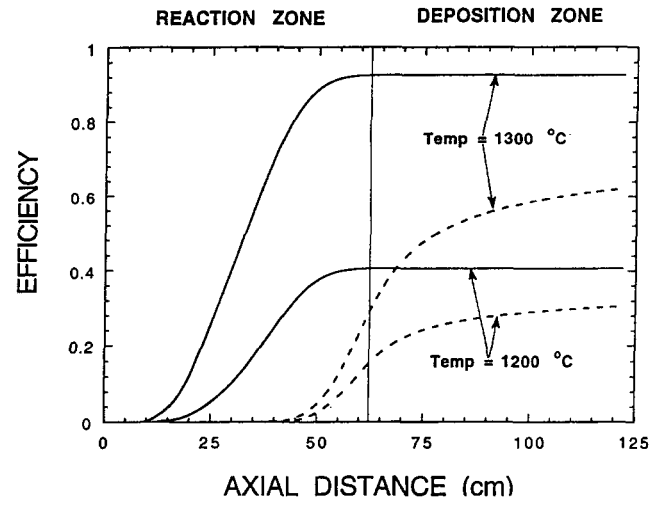

Figure 8. $SiCl_4$ conversion (solid lines) and deposition efficiency (dashed lines) along the axial distance for various furnace set temperatures.

$C_i = 0.5$ mol %; $Q = 4$ L/min.

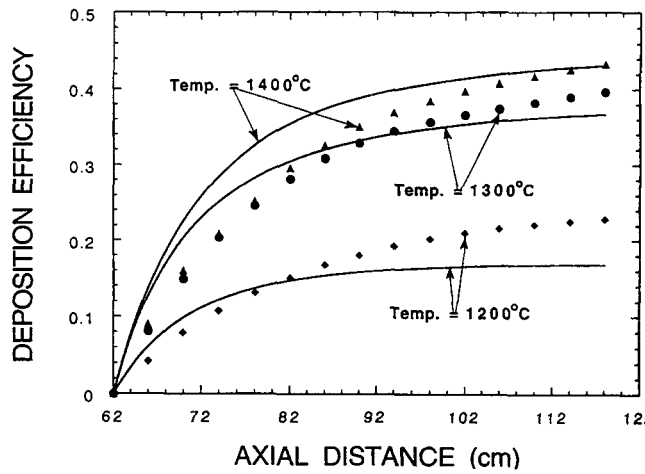

Figure 9. Deposition efficiency in deposition zone along the axial distance for various furnace set temperatures.

Experimental results (marks); theoretical results (solid lines) ($C_i = 0.5$ mol %; $Q = 4$ L/min).

is observed to be lower than $E_{DZ,\text{the}}$ at the beginning of the deposition zone, while $E_{DZ,\text{exp}}$ is higher than $E_{DZ,\text{the}}$ at the end of the deposition zone, where those particles which were pushed towards the tube center by natural convection are deposited.

Effects of inlet $SiCl_4$ concentrations on deposition efficiencies

The $SiCl_4$ conversion and deposition efficiency (E_D) for inlet $SiCl_4$ concentrations of 0.5 mol % and 5 mol % were shown along the reactor in Figure 10. The $SiCl_4$ conversion with 5 mol % increases rapidly because of the abrupt increase in gas temperature by the significant heat of reaction, but the amount of $SiCl_4$ diffused from the tube center towards the tube wall decreases because of short diffusion time during heating in the reaction zone. The overall deposition efficiency is the combined effects of $SiCl_4$ diffusion and thermophoresis, and the overall deposition efficiency with 5 mol % is lower than with 0.5 mol %. The $E_{DZ,\text{the}}$ was compared with $E_{DZ,\text{exp}}$ in Figure 11 for various inlet $SiCl_4$ concentrations and both results are in close agreement. The $E_{DZ,\text{exp}}$ decreases from 40% to 29% as the inlet $SiCl_4$ concentration increases from 0.5 mol % to 5 mol %, because the amount of $SiCl_4$ diffused from the tube center towards the tube wall decreases.

Effects of total gas-flow rates on deposition efficiencies

The $SiCl_4$ conversion and deposition efficiency (E_D) for various total gas-flow rates were shown along the reactor in Figure 12. The gas stream doesn't have enough residence time for heating at high gas-flow rates, and the $SiCl_4$ conversion decreases from 100% to 73% as total gas-flow rate increases from 2 L/min to 5 L/min. At high gas-flow rates, cooling of gas stream and deposition by thermophoresis is not complete in the deposition zone. The overall deposition efficiency decreases as total gas-flow rate increases by the combined effects of incomplete reaction and deposition. The $E_{DZ,\text{the}}$ was compared with $E_{DZ,\text{exp}}$ in Figure 13 for various total gas-flow rates. The conversion of $SiCl_4$ at $Q = 5$ L/min is lower than at $Q = 4$ L/min, and the deposition efficiency in the deposition zone (E_{DZ}) with $Q = 5$ L/min is lower than with $Q = 4$ L/min. The results of $E_{DZ,\text{the}}$ are in good agreement with $E_{DZ,\text{exp}}$ for $Q = 5$ L/min and 4 L/min. For $Q = 2$ L/min, the simulation results show that the $SiCl_4$ conversion is complete, but some particles are already deposited at the end of the reaction zone ($40 \leq z < 62$) (Figure 12), and $E_{DZ,\text{the}}$ with $Q = 2$ L/min is lower than with $Q = 4$ and 5 L/min. On the other hand, the effect of natural convection is most significant at low gas-flow rates (Kays and Perkins, 1985) and a significant amount of SiO_2 particles are believed to be pushed toward the tube center by natural convection in the experi-

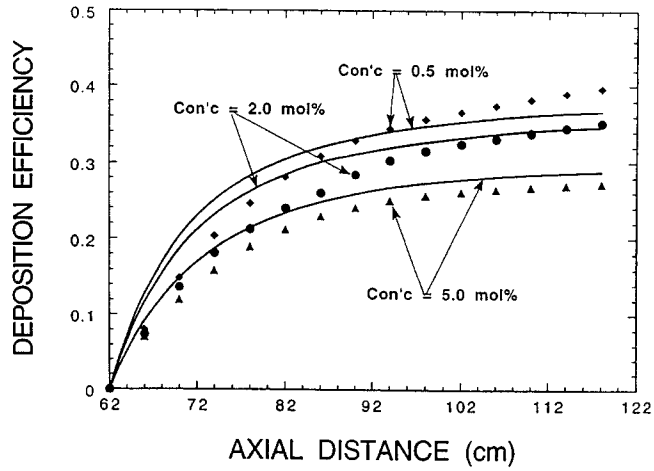

Figure 11. Deposition efficiency in deposition zone along the axial distance for various inlet $SiCl_4$ concentrations.

Experimental results (marks); theoretical results (solid lines) ($T_{ws} = 1{,}300$°C, $Q = 4$ L/min).

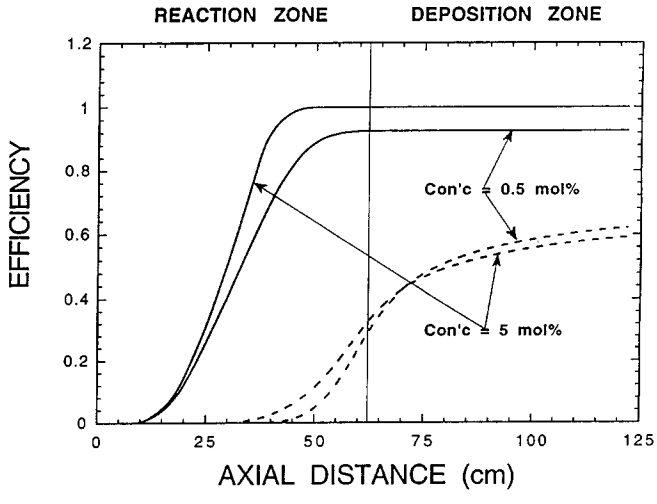

Figure 10. $SiCl_4$ conversion (solid lines) and deposition efficiency (dashed lines) along the axial distance for various inlet $SiCl_4$ concentrations.

$T_{ws} = 1{,}300$°C; $Q = 4$ L/min.

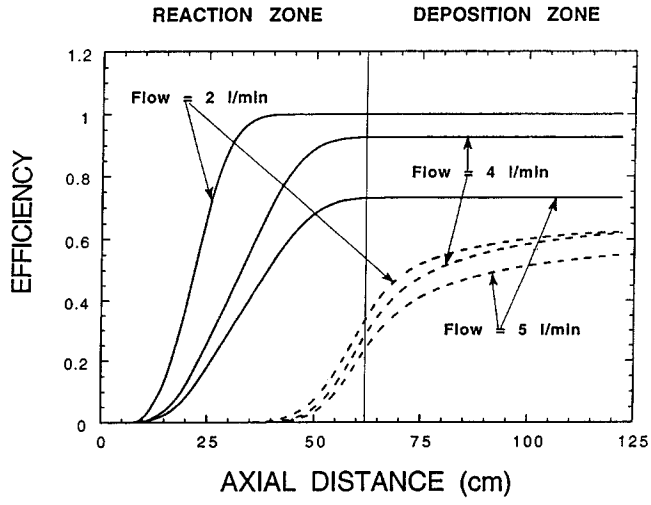

Figure 12. $SiCl_4$ conversion (solid lines) and deposition efficiency (dashed lines) along the axial distance for various total gas-flow rates.

$T_{ws} = 1{,}300$°C, $C_i = 0.5$ mol %.

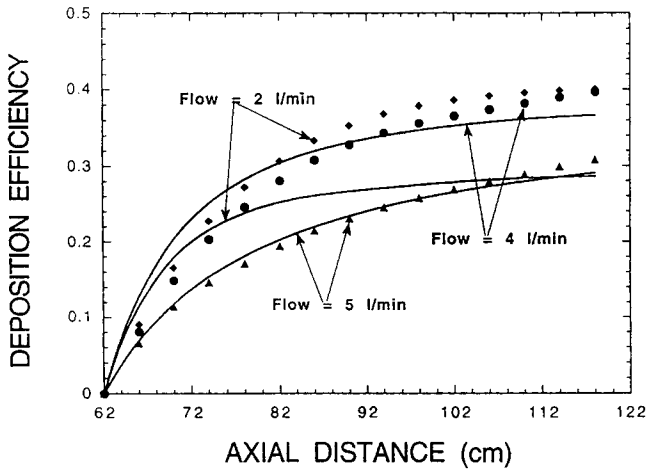

Figure 13. Deposition efficiency in deposition zone along the axial distance for various total gas-flow rates.

Experimental results (marks); theoretical results (solid lines) (T_{ws} = 1,300°C; C_i = 0.5 mol %).

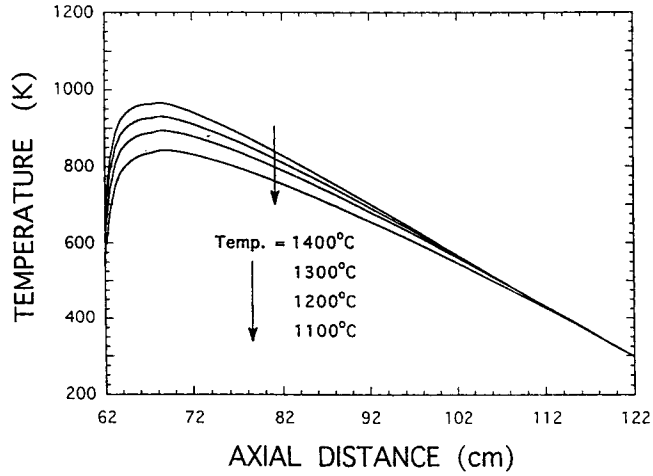

Figure 14. Controlled temperature profiles in deposition zone to deposit SiO_2 particles in uniform thickness for various furnace set temperatures.

C_i = 0.5 mol %; Q = 4 L/min.

ment with $Q = 2$ L/min. Most of these particles are deposited by thermophoresis in the deposition zone, instead of at the end of the reaction zone, and the $E_{DZ,\text{exp}}$ is observed to be higher than the $E_{DZ,\text{the}}$ with $Q = 2$ L/min.

Controlled deposition of SiO_2 particles in deposition tube

The deposition flux in the deposition zone can be made uniform by controlling the tube wall temperature profile, and uniform coating of SiO_2 particles on the deposition tube can be obtained. The following conditions for tube wall temperature should be satisfied for uniform coating in the deposition zone

$$\text{Deposition flux at } z = 2\pi K \nu \left(r M_1 \frac{\partial \ln T}{\partial r} \right)\Bigg|_{r=R} \quad \text{at } z$$

$$= \left(\frac{E_{DZ}}{L_{DZ}} \right) (1{,}000 C_i Q v^*)$$

$$= \text{constant for uniform coating} \quad (7)$$

The tube wall temperature at the beginning of the deposition zone is assumed to be the same as the temperature at the end of the reaction zone. At first, a value of E_{DZ} was assumed and, for every step in numerical integration, the tube wall temperature was calculated so that the condition of constant deposition flux (Eq. 7) is satisfied everywhere in the deposition zone. The E_{DZ} was determined by trial-and-error by assuming that the tube wall temperature at the end of the deposition zone is 25°C.

Figure 14 shows the tube wall temperature profiles for uniform coating in the deposition zone for various furnace set temperatures. At the beginning of the deposition zone, more particles are located in the region near the tube wall than near the centerline and, for uniform coating, it is required to retard the deposition rate by increasing the tube wall temperature. As the axial distance in the deposition zone increases, the tube wall temperature should be lowered to keep the temperature gradient constant for uniform coating. As the furnace set temperature increases, the gas stream is heated to a higher temperature and the tube wall temperature should be kept high to make the temperature gradient constant at the tube wall. The tube wall temperature profiles in the deposition zone for uniform coating are shown in Figure 15 for various total gas-flow rates. At high gas-flow rates, a higher fraction of SiO_2 particles are formed near the tube wall and these particles are easily deposited at the beginning of the deposition zone. The tube wall temperature should be kept high at higher gas-flow rates, to retard the deposition rates for uniform coating.

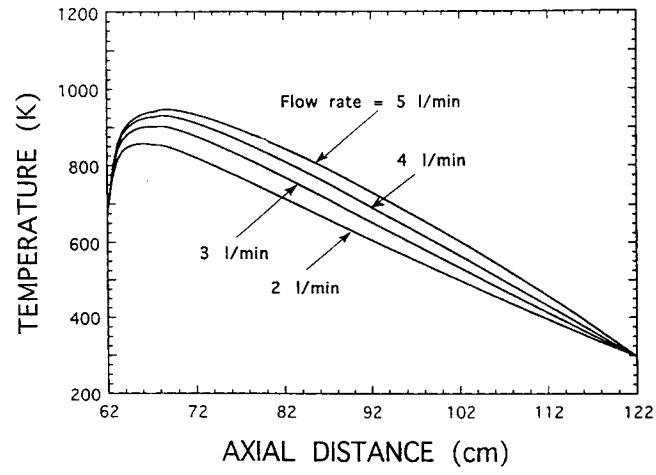

Figure 15. Controlled temperature profiles in deposition zone to deposit SiO_2 particles in uniform thickness for various total gas-flow rates.

T_{ws} = 1,300°C, C_i = 0.5 mol %.

Conclusions

The theoretical and experimental analysis of SiO_2 particle generation and deposition is presented using a tube furnace reactor. The model equations such as energy and $SiCl_4$ balance equations and aerosol dynamic equation of SiO_2 particles were solved numerically, and $SiCl_4$ conversion and deposition efficiencies were calculated. The deposition efficiencies in the deposition zone were observed in experiments as a function of axial distance by measuring the amount of SiO_2 particles deposited on the unit cells. The effects of process variables such as furnace set temperatures, inlet $SiCl_4$ concentrations, and total gas-flow rates were investigated. The experimental results of deposition efficiencies were in good agreement with the theoretical predictions. The tube wall temperature profiles to control the particle deposition for uniform coating in the deposition tube were proposed. Some key findings are summarized as follows:

(1) The $SiCl_4$ conversion increases, as furnace set temperature increases, as inlet $SiCl_4$ concentration increases or as total gas-flow rate decreases.

(2) The deposition efficiency decreases, as the furnace set temperature decreases in the region below 1,300°C because of low $SiCl_4$ conversion. As the furnace set temperature increases above 1,300°C, the $SiCl_4$ oxidation is almost complete and deposition efficiency in the deposition zone increases by the greater thermophoretic transport rate.

(3) As the inlet $SiCl_4$ concentration increases, the gas stream is heated rapidly by the significant heat of reaction and the amount of $SiCl_4$ diffused from the tube centerline towards the tube wall decreases. The deposition efficiency at high inlet $SiCl_4$ concentration becomes lower than at low inlet $SiCl_4$ concentration.

(4) The $SiCl_4$ conversion and deposition efficiency decrease as total gas-flow rate increases above 4 L/min, because of the incomplete oxidation and deposition. The effect of natural convection becomes significant at $Q = 2$ L/min, and more particles are formed in experiments near the tube center by natural convection than by theoretical prediction. The $E_{DZ,\exp}$ becomes greater than $E_{DZ,\text{the}}$.

(5) The proposed tube wall temperature profiles in the deposition zone for uniform coating increase at the beginning of the deposition zone and decrease later, to keep the deposition flux constant. As the furnace set temperature increases, and as the total gas-flow rate increases, the tube wall temperature profiles in the deposition zone for uniform coating increase.

Acknowledgments

Part of this study was supported by Korean Ministry of Education through Research Fund for New Materials.

Notation

C = concentration of $SiCl_4$, mol/cm^3
C_i = inlet concentration of $SiCl_4$, mol/cm^3
C_p = heat capacity of O_2, J/g·K
D = diffusivity of $SiCl_4$ for O_2, cm^2/s
D_p = diffusivity of SiO_2, cm^2/s
E = activation energy for oxidation of $SiCl_4$, J/mol, kJ/mol
ΔH = heat of reaction for $SiCl_4$ oxidation, cal/mol, kJ/mol
k_0 = preexponential Arrhenius rate constant, s^{-1}
K = thermophoretic coefficient
L_{DZ} = length of deposition zone, cm
M_q = qth order moment
n = particle-size distribution function
N_{av} = Avogadro's number
P_{eh} = Peclet number for energy transfer, $2RU/\alpha$
P_{em} = Peclet number for $SiCl_4$ mass transfer, $2RU/D$
Q = total gas-flow rate at STP, L/min
R = radius of reactor, cm, 2.2 cm
r = radial distance of reactor, cm
RXN = oxidation rate of $SiCl_4$, mol/cm^3·s, $-k_0 \exp(-E/RT)C$
T = gas temperature, K
T_i = inlet gas temperature, K, 298 K
T_{ws} = furnace set temperature, K
u = axial velocities of gas stream, $u = 2U[1-(r/R)^2]$, cm/s
U = average gas velocity, cm/s
v, v' = particle volume, cm^3
v_g = geometric mean volume of SiO_2 particle, cm^3
v^* = volume of SiO_2 monomer, cm^3
z = axial distance of reactor, cm
α = thermal diffusivity, cm^2/s
β = collision frequency function
δ = Dirac delta function
μ = viscosity of gas stream, g/cm·s
ν = kinematic viscosity, cm^2/s
ρ = density of O_2, g/cm^3
σ = standard deviation

Literature Cited

Akhtar, M. K., Y. Xiong, and S. E. Pratsinis, "Vapor Synthesis of Titania Powder by Titanium Tetrachloride Oxidation," *AIChE J.*, **37**, 1561 (1991).

Akhtar, M. K., S. Vermury, and S. E. Pratsinis, "Competition between $TiCl_4$ Hydrolysis and Oxidation and Its Effect on Product TiO_2 Powder," *AIChE J.*, **40**, 1183 (1994).

Anderson, D. A., J. C. Tannehill, and R. H. Pletcher, *Computational Fluid Mechanics and Heat Transfer*, McGraw-Hill, New York (1984).

Brock, J. R., *Simulation of Aerosol Dynamics in Theory of Disperse Multiflow*, R. E. Mayer, ed., Academic Press, New York (1983).

Chen, L., T. Goto, and T. Hirai, "Preparation of Silicon Carbide Powders by Chemical Vapour Deposition of the SiH_4-CH_4-H_2 System," *J. Materials Sci.*, **24**, 3824 (1989).

French, W. G., L. J. Pace, and V. A. Foertmeyer, "Chemical Kinetics of the Reactions of $SiCl_4$, $SiBr_4$, $GeCl_4$, $POCl_3$ and BCl_3 with Oxygen," *J. Phys. Chem.*, **82**, 2191 (1978).

Friedlander, S. K., *Smoke, Dust and Haze*, Wiley, New York (1977).

IMSL, *IMSL Contents Document*, 8th ed., Int. Math. and Statist. Libraries, Houston (1980).

Kays, W. M., and H. C. Perkins, *Handbook of Heat Transfer*, W. M. Rohsenow, J. P. Hartnett, and E. N. Ganic, eds., Chapter 7, McGraw-Hill, New York (1985).

Kim, K. S., and S. E. Pratsinis, "Manufacture of Optical Waveguide Preforms by Modified Chemical Vapor Deposition," *AIChE J.*, **34**, 912 (1988).

Kimura, I., N. Hotta, H. Nukui, N. Saito, and S. Yasukawa, "Particulate Characteristics and Deposition Features of Fine AlN Powder Synthesized by Vapor-Phase Reaction," *J. Mater. Sci.*, **24**, 4076 (1989).

MacChesney, J. B., P. B. O'Connor, and H. M. Presby, "A New Technique for Preparation of Low-Loss and Graded Index Optical Fibers," *Proc. IEEE*, **62**, 1278 (1974).

Morooka, S., T. Yasutake, A. Kobata, K. Ikemizu, and Y. Kato, "Mechanism of TiO_2 Fine Particle Formation and by Gas-Phase Reaction," *Kagaku Kogaku Ronbunshu*, **13**, 159 (1987).

Nagel, S. R., J. B. MacChesney, and K. R. Walker, "An Overview of the Modified Chemical Vapor Deposition (MCVD) Process and Performance," *IEEE J. Quantum Electron.*, QE, **18**, 459 (1982).

Okuyama, K., Y. Kousaka, N. Tohge, S. Yamamoto, J. J. Wu, R. C. Flagan, and J. H. Seinfeld, "Production of Ultrafine Metal Oxide Aerosol Particles by Thermal Decomposition of Metal Alkoxide Vapors," *AIChE J.*, **32**, 2010 (1986).

Okuyama, K., R. Ushio, Y. Kousaka, R. C. Flagan, and J. H. Seinfeld, "Particle Generation in a Chemical Vapor Deposition Process with Seed Particles," *AIChE J.*, **36**, 409 (1990).

Powers, D. R., "Kinetics of $SiCl_4$ Oxidation," *J. Amer. Ceram. Soc.*, **61**, 295 (1978).
Pratsinis, S. E., T. T. Kodas, M. P. Dudukovic, and S. K. Friedlander, "Aerosol Reactor Design: Effect of Reactor Type and Process Parameters on Product Aerosol Characteristics," *Ind. Eng. Chem. Process Des. Dev.*, **25**, 634 (1986).
Pratsinis, S. E., and K. S. Kim, "Particle Coagulation, Diffusion and Thermophoresis in Laminar Tube Flows," *J. Aerosol Sci.*, **20**, 101 (1989).
Seinfeld, J. H., *Atmospheric Chemistry and Physics of Air Pollution*, Wiley, New York (1986).
Simpkins, P. G., S. Greenberg-Kosinski, and J. B. MacChesney, "Thermophoresis: The Mass Transfer Mechanism in Modified Chemical Vapor Deposition," *J. Appl. Phys.*, **50**, 5676 (1979).
Suyama, Y., and A. Kato, "Effect of Additive on the Formation of TiO_2 Particles by Vapor Phase Reaction," *J. Amer. Ceram. Soc.*, **68**, C154 (1985).
Walker, K. L., G. M. Homsy, and F. T. Geyling, "Thermophoretic Deposition of Small Particles in Laminar Tube Flow," *J. Colloid Interf. Sci.*, **69**, 138 (1979).
Walker, K. L., F. T. Geyling, and S. R. Nagel, "Thermophoretic Deposition of Small Particles in the Modified Chemical Vapor Deposition (MCVD) Process," *J. Amer. Ceram. Soc.*, **63**, 552 (1980).

Manuscript received Oct. 28, 1996, and revision received Apr. 21, 1997.